Lab report
E217 STYX

Chenhuan Wang and Harilal Bhattarai

November 18, 2020

In this experiment, we learnt about basic nuclear electronic, gas detectors, and tracking system of charged cosmic radiation. The goal of the experiment is to obtain the angular distribution of atmospheric muons. To do so, we determined and set up the operation voltage 2150 V for PMT and 2.0 V as threshold voltage. In the end, we found that the muon angular distribution deviate quite significantly away from theoretical $\cos^2\theta$ curve.

1. Introduction

Cosmic rays physics as a frontier to discover and validate laws of physics has existed for quite some time. As early as 1912, Victor Hess already used balloon with "electrometers" to detect ionizing radiation at an altitude [1]. Nowadays, cosmic rays is a popular research area with numerous large scale experiments, such as IceCube, AMS-02, and Pierre Auger. Although cosmic rays experiments suffer from uncontrolled particles sources, its energy (up to 1×10^{20} eV) exceeds state-of-art accelerator energy (up to 13 TeV) by a large margin [2].

A large portion of cosmic rays consists of neutrinos, which have a tons of unsolved mysteries, like neutrino oscillations, origin of its mass and $\mathcal{CP}$ (even $\mathcal{CPT}$ violation [3]) violations. By studying energy spectrum of comic rays, we can look into the propagation of these particles and thus determine properties of intergalactic space [2]. Sometimes features of cosmic rays might need dark matter to make sense [4][5].

Beside all these potential intriguing problem, the setup of Styx has a rich heritage. The straw modules were formerly a part of ZEUS Straw Tube Tracker (STT) to study secondary cosmic rays [6]. Thus this experiment also allows us to look back into history and appreciate early generation's contribution to physics.

This report is arranged as following. A general overview of cosmic rays is given in section 2. Electronics and schematics of the setup are shortly introduced in section 3. Before the data taking, optimal operating voltage PMT and threshold of discriminators need to be set and straws should be calibration. These are done in sections 4 and section 5. The tracking analysis is presented in section 6. Section 7 concludes this report.

2. Cosmic rays

Cosmic rays are a population of elementary particles and nuclei coming from outer space with several MeV to macroscopic energies ($\sim$ J). Energy spectra of cosmic rays follow a falling power-law (albeit with several small features) [7] [2]

$$N(E) \propto E^{-\gamma}$$

Cosmic rays of primary origin (i.e. directly from astrophysical sources without interactions) enter the earth atmosphere and they will produce the so-called secondary cosmic rays. Comparing the interaction lengths for hadronic and leptonic particles and atmosphere column density reveals that practically all cosmic rays at sea level are secondary, even tertiary [4]. All primary particles either interaction with air or decay depending on their energies. Essentially the atmosphere acts like a giant calorimeter and particle cascades are generated [4].

Most of primary cosmic rays consist of hydrogen atoms [2]. In fact, 85% are protons [4]. These protons produce mainly secondary pions and then kaons. In the end, at sea level most abundant particles with energy $> 1\,\mathrm{GeV}$ are muons (and corresponding neutrinos) [7].

There is a rather important angle dependence of muon spectra because of competition between decay and interaction. At sea level, the muon population is dominated by low energy muons (generally true for all particles). With low energy, it becomes easier for muons from inclined angle to decay and absorbed in atmosphere [4]. This can be parametrized as [4]

$$I_\mu(\theta) = I_\mu(\theta = 0) \cos^n \theta \tag{1}$$

with $n \approx 2$. Note that this formula is valid only for small zenith angle [8]. Physically, it can be understood as we still expect some muon flux at $\theta = \pi/2$ but equation 1 predicts zero muon flux.

Energetic particle will produce extensive shower in the atmosphere. This makes electrons and positrons quite abundant at sea level. They usually have pretty low energy, because of production mechanisms and energy losses [4].

3. Setup

3.1. Individual components

Drift chamber is a type of gaseous ionization detector. As its name suggests, it detects ionizing particles by a electric field inside. When the gas atoms get ionized, the electron will move to the anode and generate a signal. Especially near the anode wire, the electric field is so huge that the electron becomes ionizing itself and cause further discharge. This effect is called avalanche [9]. Obviously, number of ions collected at anode depends strongly on the voltage put between anode and cathode.

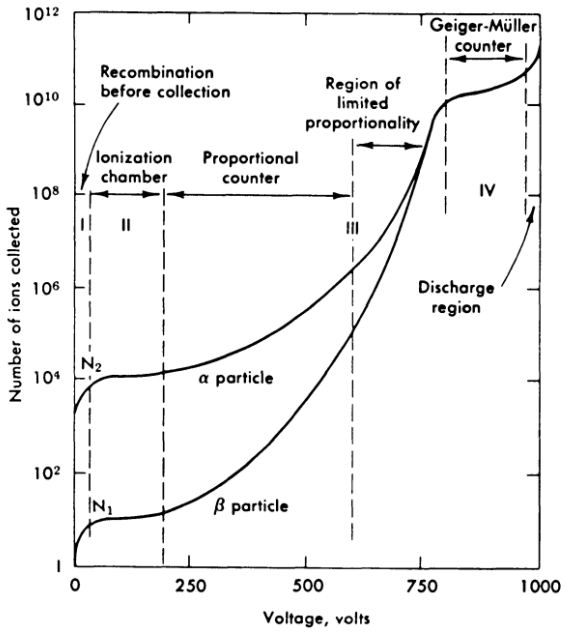

Figure 1: Example diagram of number of ions versus applied voltage in a single wire gas chamber (taken from [9]). Note that vertical axis is in logarithmic scale.

An exemplar development of number of ions with increasing voltage is shown in figure 1. In this setup, we essentially want to saturate the gas chamber (thus to region IV in figure 1) so that it can reliably count the ionizing particles regardless of their energy.

In this experiment, there are three drift chamber modules, see figure 3. In each of these, there are three layers of 88 straws [10].

Scintillator and PMT work as external triggers here. They together are able to convert ionizing particle into relatively low energy photons (scintillator), convert photon into electrons using photoelectric effect, and finally with electric field to multiply the number of electrons to generate visible signals [11]. Here two such detectors are used, one on top of the drift chamber and on below [10], see figure 3.

Shaper A shaper is a module which turns inputs pulse into logic signals of standard levels and fixed width [9].

TDC stands for Time-to-Digital Converter measures the time between two signals and gives the time difference of these two [9].

Coincidence unit determines if two or more logic signals overlap with each other within a preset time intervals and output signal if true and no signal if false. The present time is called resolving time. It can be implemented with a transmission gate or simply summing and passing through a discriminator [9].

3.2. Whole setup

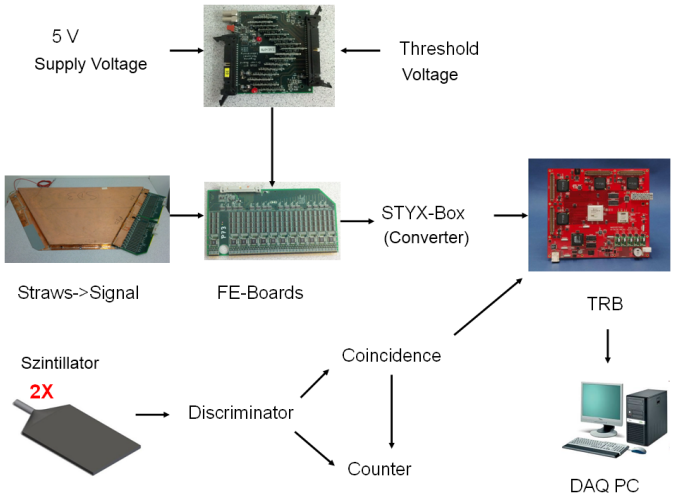

Figure 2: Schematics of the experiment setup [10].

Schematically the setup is like in figure 2. The front end boards (FE-boards) are attached to the straws. The boards contain amplifiers, shapers and discriminators, so that as long as input signal pass a set threshold, a logic signal is generated. The threshold voltage can be set on an external power supply. As for the trigger part, the signal will need to pass discriminators (to filter out noises) and goes to a coincidence unit. The coincidence unit makes sure that an event is only recorded when it flies through both scintillators. In the end, signals from straw modules and scintillator units go into TRB board and to the PC [10].

The actual setup is shown in figure 3. Straw modules with FE-boards are the copper layer between the two plastic bags, which are the triggers. Several other electronics are on the rack on the right side of figure 3.

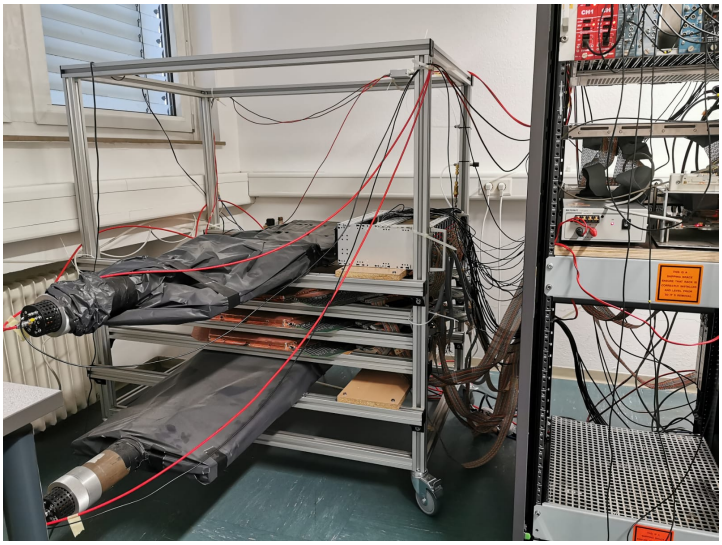

Figure 3: The actual setup

4. Voltage determination

As first thing, we check the gas system. There are bubbles coming out every few seconds at window on a test tube, it is clear that the gas system was working. Then we need to determine voltages of PMTs and discriminator.

4.1. PMT operation voltage determination

As mentioned in section 3.1, behaviour of drift chamber strongly depends on voltage applied between anode and cathode. Thus to make sure PMTs are working properly, voltages need to be set accordingly. To determine the PMT operation voltages we have three counters. They show the number of events in 10 s interval of top PMT, bottom PMT, and coincidence of these two.

We start by varying the voltage for bottom panel from 1700 V to 2300 V in steps of 50 V. Four measurements at every 10 second with every step of 50 V and calculate their averages to reduce the statistical errors. After measuring rate, we plot a graph between average rate against number of counts. Errors of "count rates" are estimated using Poisson distribution. In figure 4 we can see that initially the count rate increases quite steeply with the voltage. Then it start to get saturated from 2000 V and flattens out from 2100 V. In the this region, a linear fit is done. We see that data points with voltages less or equal to 2050 V don't follow this linear fit anymore. Therefore. According to [10], we took a working point at starting point of the plateau, thus 2100 V.

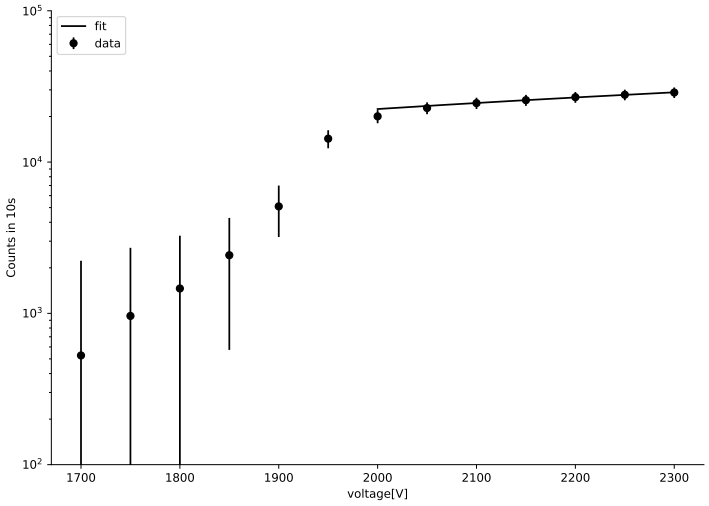

Figure 4: The number of counts for bottom panel with varying voltage. Vertical axis is in log scale. Raw data are in appendix.

With bottom PMT voltage at 2100 V, we vary the voltage for top panel as in before step in the same range. We measure the coincidence rate via its counter. Unfortunately, the rightmost counter is slightly broken, the last digit of count number is not clearly readable. It could lead some statistical error, but in the end it is not very significant. By plotting a graph of coincidence rate over, we have again a plateau curve 5. From figure 5 we see that initially

coincidence rate increases with voltage then it has a clear plateau. 2150 V is the point the curve starts to be flat and it is a good working point for the PMT.

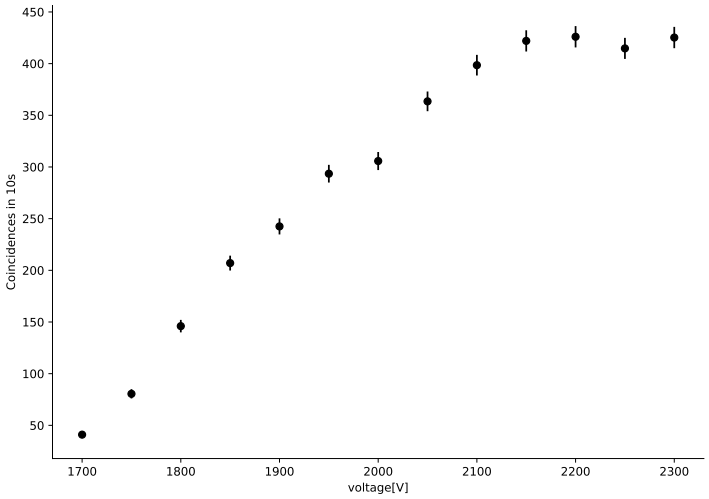

Figure 5: The number of counts for top panel with varying voltage.Raw data are in appendix.

4.2. Determination of the front-end threshold voltage

We have to determine the optimal voltage for the discriminator. The voltage is adjusted using power supply [10]. To determine its appropriate value, we processed with `StyxM2C2` along with the raw data. Here, we have taken 25 000 events in every step of 0.3 V from 1.4 V to 2.6 V. Then to do find good channels a closer look into the `root` files is necessary. Finally, we compared the different voltage settings using `StyxThresholdScane`.

To choose threshold voltage, first of all, we look at the rates files two of them are in fig 6. The hits in channel decreases with increasing voltage. At low voltages (low threshold) there are plenty of noises and at high voltage some of the signals are cut. So we indeed expect decreasing curves in rate files. Thus we say that roughly the optimal voltage should be in the middle. Its exact value needs still to be determined later.

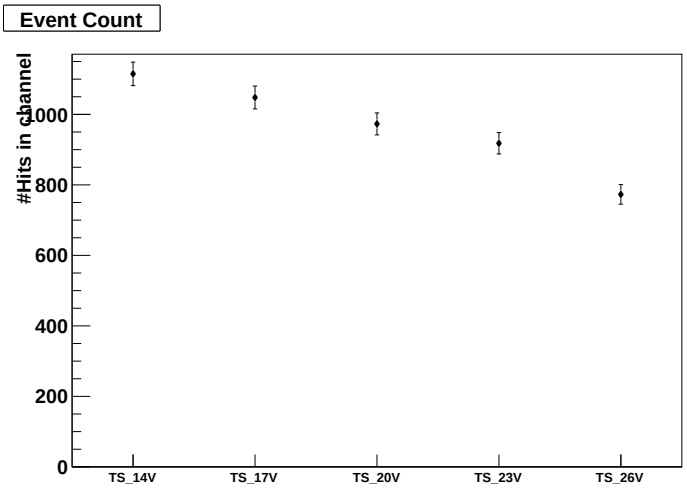

(a) At TDC 1 channel 2.

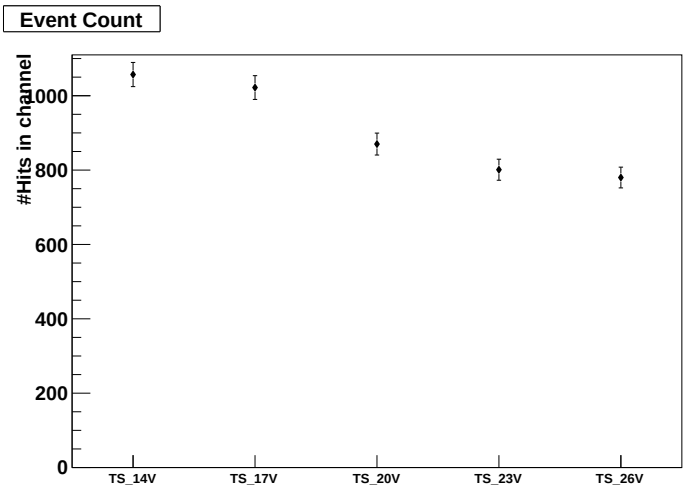

(b) At TDC 1 channel 5.

Figure 6: The rate plots in TDC 1 channel 2 and TDC 1 channel 5 at different voltages.

Now we compare the overlay plots of different channels and TDCs. Two examples are in fig 7. It shows number of hits in six straws at different voltages. In figure 7, the peaks are for different straws and horizontal axis is in time which has something to do with electronics of the setup [10]. We see that the noise level is too high at low voltages and thus heights of these peaks are quite different. Peaks at 2.0 V seems quite uniform for all straws, but not for other voltages. We want to find the lowest voltage so that the peaks seem to be of the same heights. Therefore we choose the threshold voltage is 2.0 V.

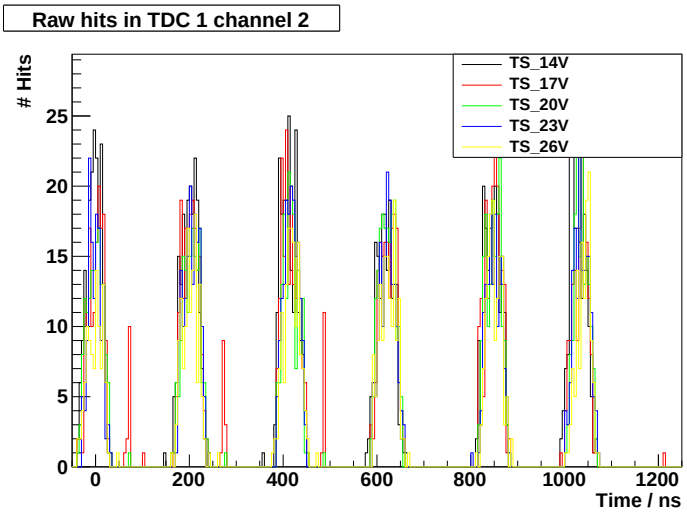

(a) In TDC 1 channel 2 at different voltages.

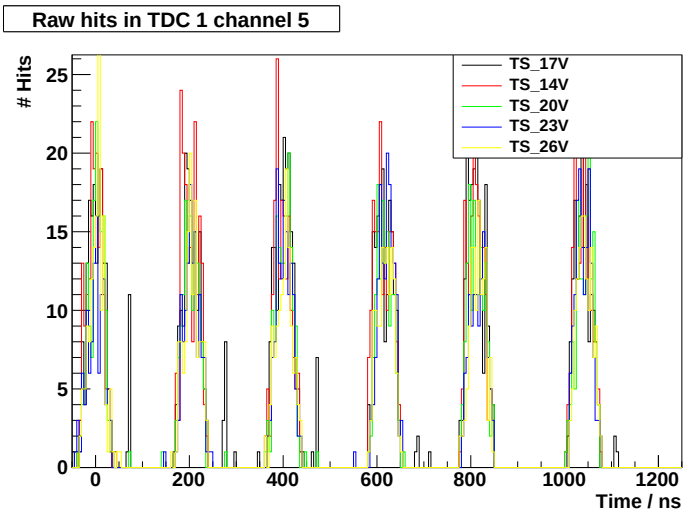

(b) In TDC 1 channel 5 at different voltages.

Figure 7: The overlay file of time-multiplexed vs hits

5. Calibration

After adjusting the PMT voltage and threshold voltage, the setup should function as expected. An overnight data taking is performed and all data has been stored. The tutor mentioned that the calibration option 1 is not working properly, so the second option is chosen.

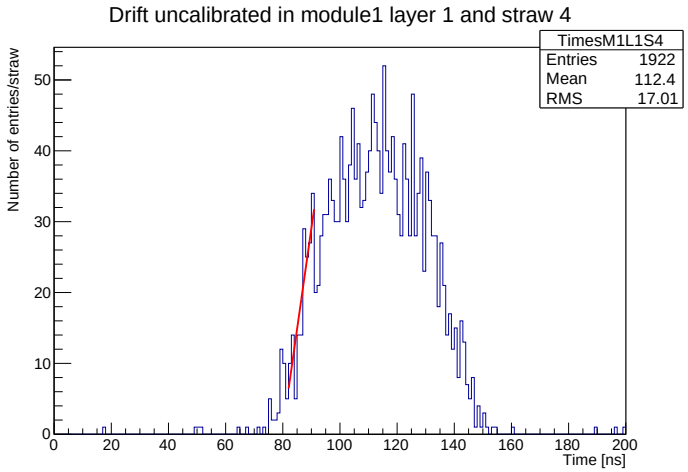

(a) Before calibration. Red line is a fit.

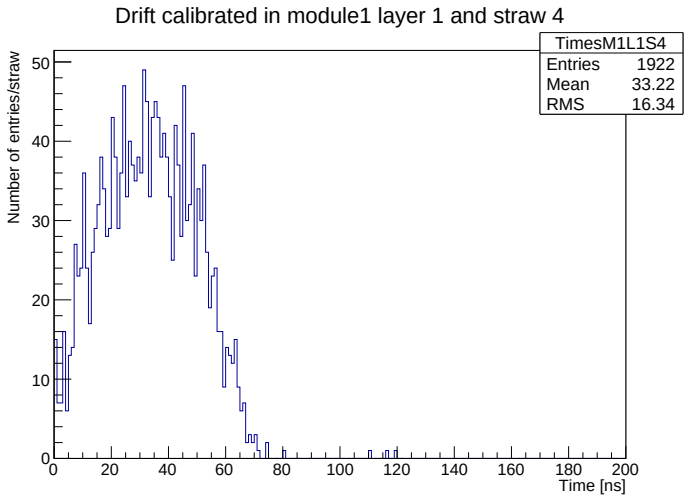

(b) After calibration

Figure 8: Drift time spectrum before and after calibration.

The calibration is done straw-by-straw using the data. One part of the data is used to map out the drift time spectrum for each straw. During the calibration, the program will try to shift the drift time, so that it starts at zero time. Exemplar spectra can be found in figure 8. During the calibration a fit is done to the ”leading” edge of the drift spectrum. The initial time t_0 is then set the intersection point of the fit line with horizontal axis.

The calibration is performed with 300 000 events using the program `StyxCalibration` (with

`--no-clean` and `--all` options). The calibration method is specified with `-A CalibStrawByStraw`. After execution of the command, corresponding `root` and `txt` file are generated.

In the generated `root` file, there are two plots of particular interest: `Uncalibrated/Layers2D` and `Calibrated/Layers2D`. These plots show the drift spectra for each straw in one particular module and layer before and after calibration. Some examples are figure 9, 10, and 11.

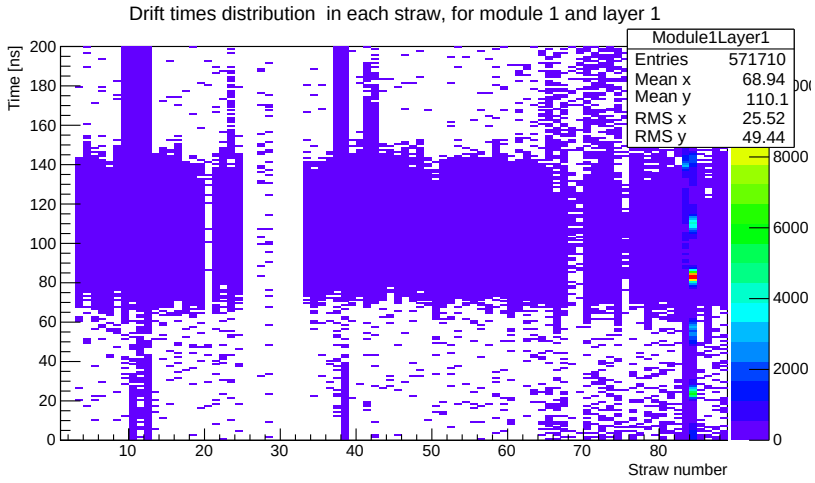

(a) Before calibration.

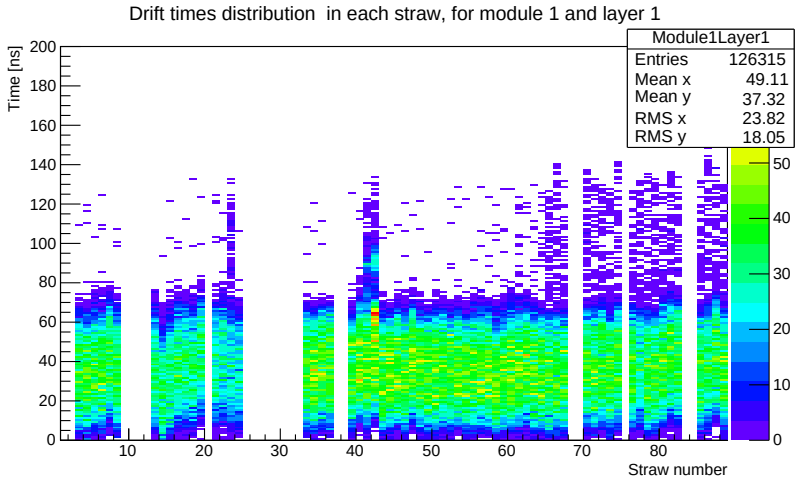

(b) After calibration

Figure 9: Drift time spectra for all straws in module 1 and layer 1 before and after calibration.

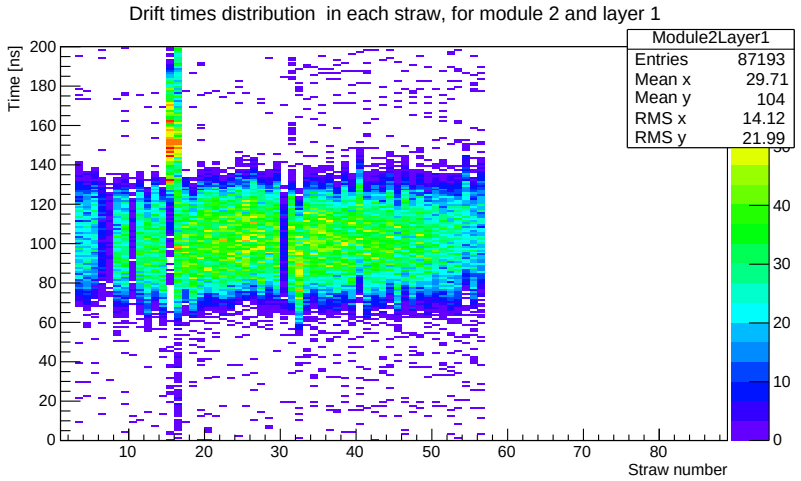

(a) Before calibration.

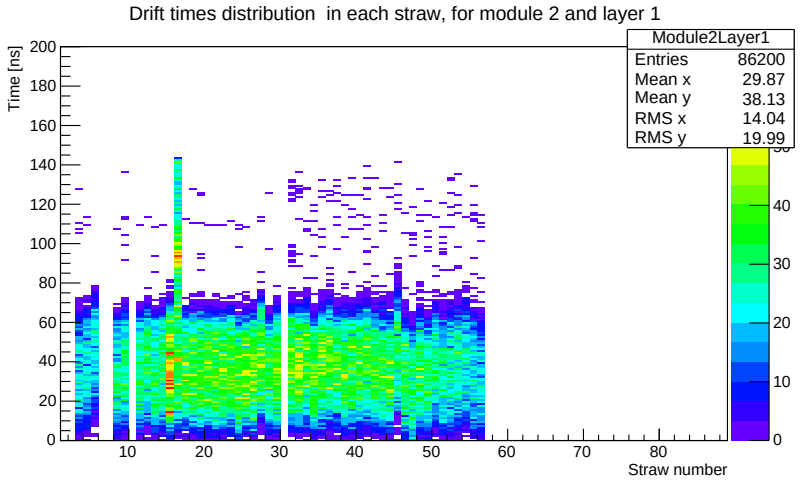

(b) After calibration

Figure 10: Drift time spectra for all straws in module 2 and layer 1 before and after calibration.

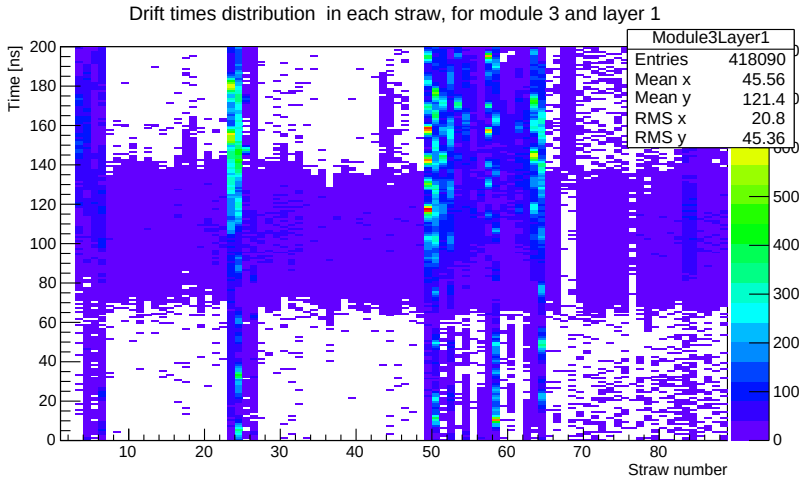

(a) Before calibration.

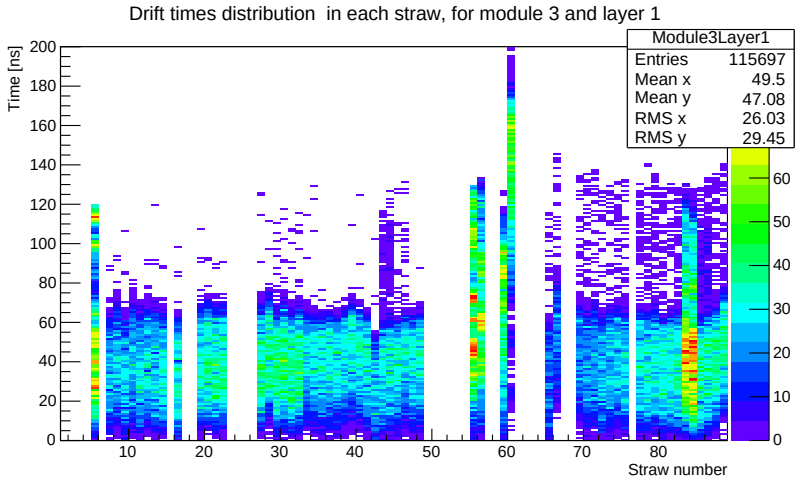

(b) After calibration

Figure 11: Drift time spectra for all straws in module 3 and layer 1 before and after calibration.

By comparison of these plots, we see that the calibration works normally for most straws. Before the calibration, there are no particular "hot" time (interval of time with clear peak in event counts) and events are rather scattered in time. But after, events are properly aligned with each other and there is a clear peak at $t \approx 40\,\text{ns}$. One can also notice that some straws don't have a lot of outputs or even no output at all. These straws should be marked as "dead". Sometimes, even after calibration, the drift spectra cannot get into the shape we expect, such as straw 15 and 16 in figure 10. This can be understood as the straws cannot be properly calibrated. The exact reason of failing calibration is still yet unknown. These certainly should not be used for the track analysis and these straws are marked as "hot" or "continuous".

The aforementioned labels to each straws can be mapped onto the cross section of the detectors, see figure 12.

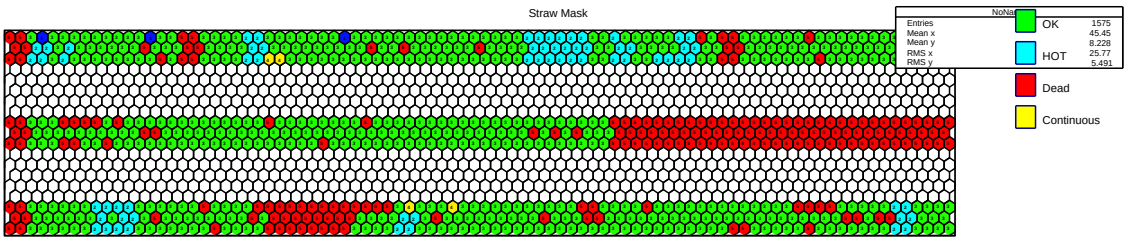

Figure 12: Straw masks. Note that the numbering should start from bottom. It means that the bottom module is module 1, the same for layer numbering. Dead straws are in orange.

With the masks, one can even simulate the events. By looking at it, we are able to gain further insight to the reconstruction process (algorithms). For example, with number of events at 20 and number of tracks at 3, one has figure 13. In the figure, red circles should be the expected position of the track only using one straw on one layer. When signals get correlated in the same module, possible tracks (green line) can be drawn. Then the signals from all three modules get combined together and a clear track (blue dotted lines) can be reconstructed.

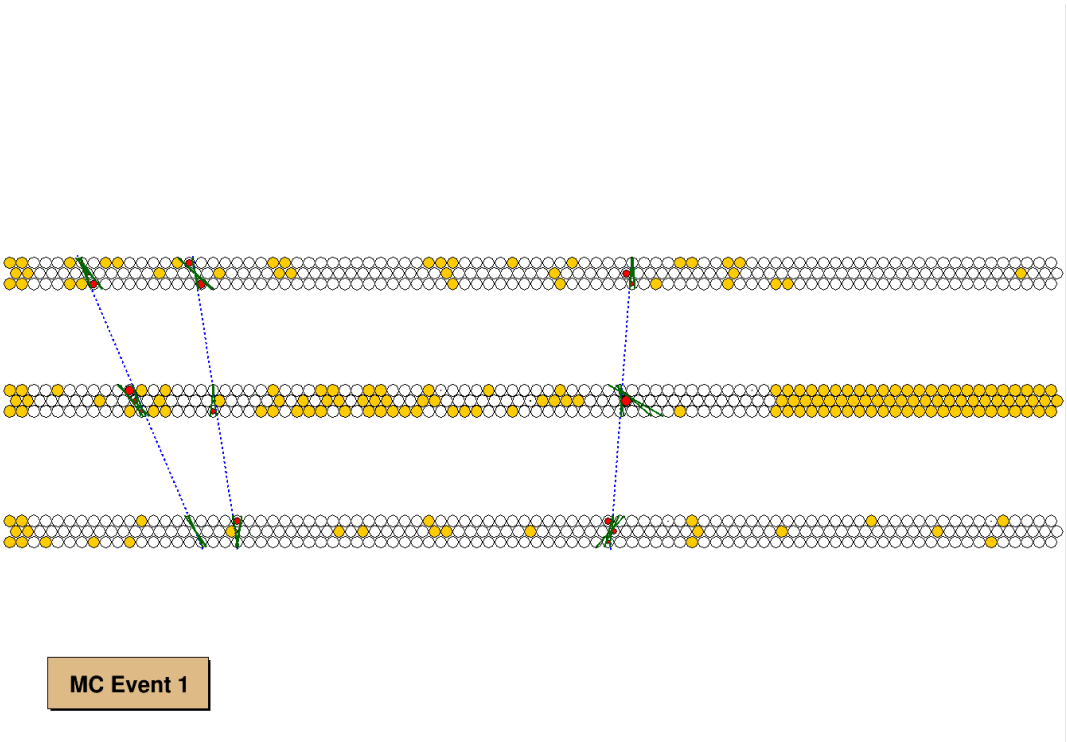

Figure 13: Simulation of events with `Nevents=20` and `Ntracks=3`. Orange straws are the straws marked as "dead".

6. Tracking analysis

Now we have the straws are calibrated with the 300 000 events, we want to reconstruct other 200 000 events with `StyxM2C2` (of course with calibration applied). These events should not overlap with each other to avoid bias. The program `StyxLabCourse` is used for the analysis. It contains a class `StudentAnalysis`, where extra code can be inserted to analyze the data. Since the its methods are called for every event, it becomes easier to store some rudimentary histograms to `root` files first and use macro to draw rather complicated histograms.

One can inspect the number of hits for each layer in one module. For example, the plot of bottom module is figure 14. It is expected that the three histograms have similar shapes, considering there physical vicinity. The shapes originate from the geometry of the detectors: some straws are just longer than others, resulting more hits.

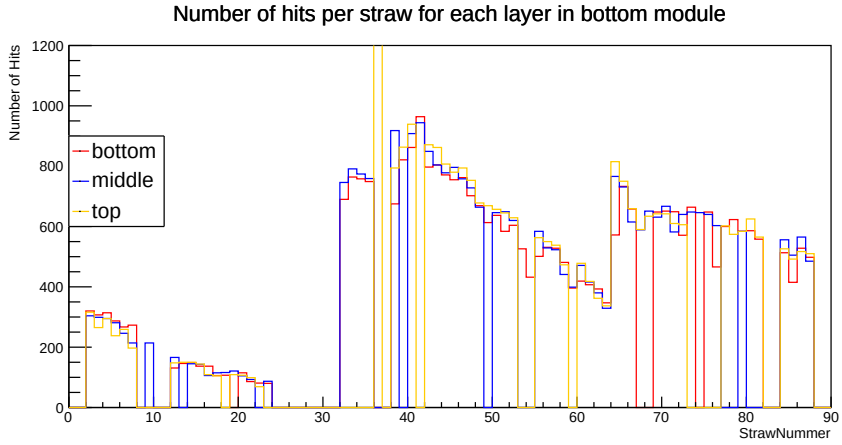

Figure 14: Number of hits per straws for each layer in bottom module

Comparison of total numbers of hits in modules is potentially interesting as well. Figure 15 shows the total number of hits in bottom and top modules. They have similar shapes in some regions, but quite different in some other regions. This can be caused by the "qualities" of straws, i.e. positions of dead and hot straws on the modules don't match each other.

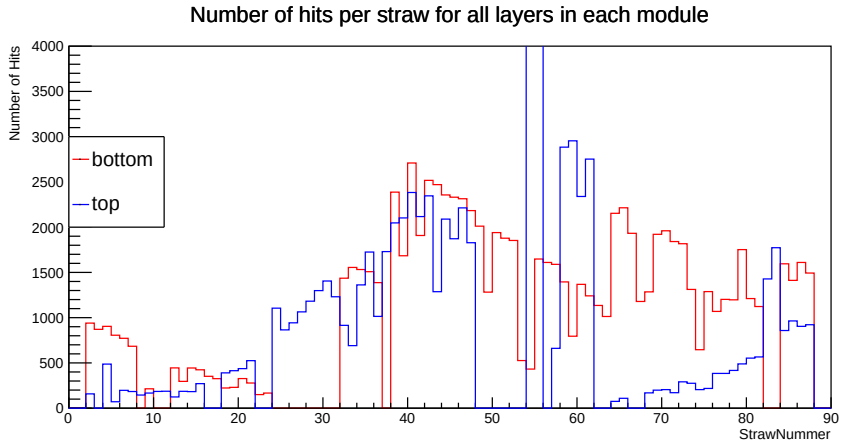

Figure 15: Number of hits per straws for all layers in bottom and top module

Figure 16 shows the correlation between number of tracks and number of hits of an event. According to [12], in `root` lower limit of a bin is included and upper limit is excluded (it becomes lower limit for the next bin).

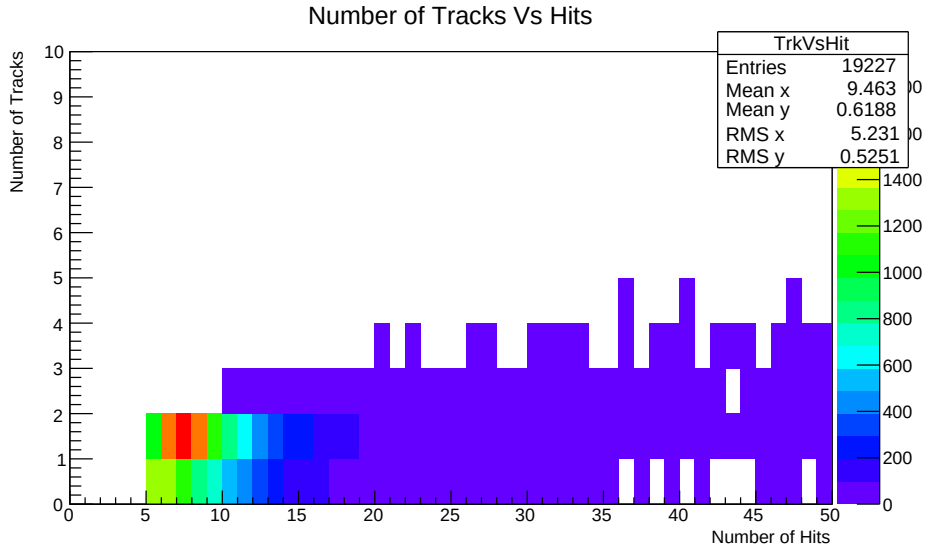

Figure 16: Number of tracks against number of hits

There are two clear sharp edges with number of hits at 5 and 10 and a couple of more subtle ones with number of hits at 20 and $\sim$ 35. Thus the interpretation of the plot in figure 16 is that the reconstruction algorithm probably demand minimal 5 hits for every track. This "rule" breaks down at high number of hits, probably because that an event with high number of tracks is not very likely.

A obvious "hot" region in figure 16 has number of tracks at 1 and number of hits ~ 7. Thus most events have only 1 track and ~ 7 hits registered. One can try to imagine the distribution projected to horizontal axis, i.e. an one-dimensional histogram of number of hits. It resembles a shape of Poisson distribution (with a lower cutoff of course), which is characteristic for a counting experiment. Unfortunately, without the programs it is hard for us to actually draw this histogram.

Angular (zenith angle) distribution of events with one track is shown in figure 17. It presumably is because of limitation of the reconstruction program that only one zenith angle can be stored for one event. This cut will not in theory create a bias in the angular distribution, since there is no reason to believe that multiple tracks in one event are correlated in any way. There is an ambiguity in the data, namely the definition of `trackSlope` used in the program. We interpreted it as the plain slope instead of the angle, so that the zenith angle is calculated with arctan function. Either way, the "choice" of the definition has virtually no impact on the angular distribution and following fit.

Basic features of figure 17 are sort of expected. It peaks at zero zenith angle, since decay probability starts to increase with the angle, see equation 1. A closer look is necessary in order to compare it with the theory. A fit is done

$$f(x) = A \cos^n x$$

between $\theta = -0.5$ and $\theta = 0.5$, since at large angle the $\cos^2 \theta$ relation does not apply anymore.

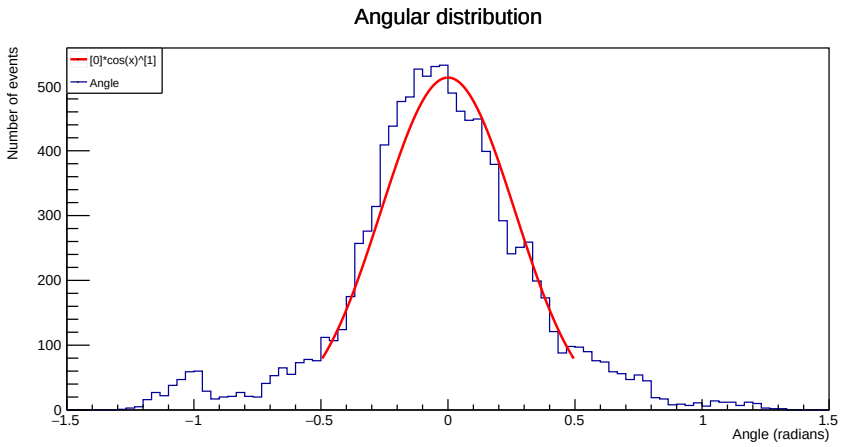

Figure 17: Angular distribution of events with a single track

A and n are the fit parameters, which are determined as

$$A = 513.00 \pm 6.95$$
$$n = 14.59 \pm 0.35$$

The interval of zenith angle can certainly be adjusted to influence the quality of the fit. But we reckon that our choice should cover the region that distribution is supposed to follow equation 1 and some changes don't really affect results too much anyway.

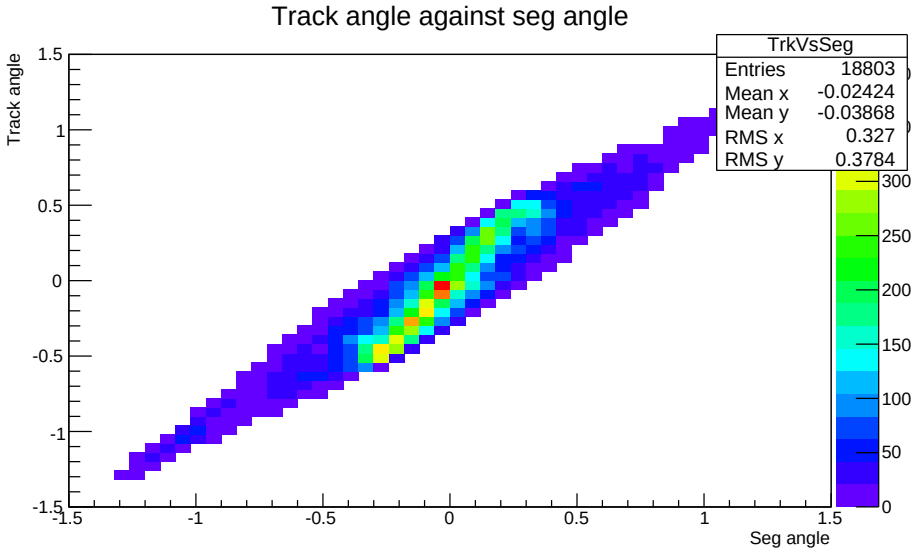

Figure 18: Zenith (track) angle against segment angle.

Another plot worth investigating is zenith angle (track angle) against segment angle for events with one track, see figure 18. Segment angle, we suppose, denotes the angle of the "track" in only one module. In theory they should match perfectly. But we need to consider detector space/angle resolution, so that the distribution is smeared. Figure 18 is almost what

we want to see, except the central "hot" regions is inclined a bit and thus the plot is not symmetric along 45° line.

7. Conclusion

After two days' effort, StyX is properly setup. Calibration masks match with number of hits per straw quite well. In other word, calibration works. But in the end, the overall result is borderline satisfactory.

Distribution of events on two-dimensional plane of segment angle and track angle is a bit odd. Ideally, we would have symmetric distribution even considering resolution. This likely has something to do with the reconstruction algorithm or even the geometry of the setup. Since both subjects are not main focus of this report, we will not go deep and try to speculate the exact problem(s).

The goal of the experiment is to obtain the angular distribution of atmospheric muons. The distribution doesn't agree with theory. The value of n deviate from the theory quite a lot ($\sim 35\sigma$ away). Statistical error can certainly be excluded. It is highly unlikely that the theory is faulty here, since some other more sophisticated and advanced experiments have $n \approx 2$ [13][8]. Then we only have setup or reconstruction method to blame. Again we are not familiar with the reconstruction so no further speculations.

The geometry of the detectors are certainly a factor here. Figure 3 shows that the trigger systems are stacked directly over and under the straw modules. One problem is that in the electronics we demand both PMT must have signals in order to record the events (coincidence). This produces a bias in the data, in the sense that once the incident angle is relatively large, the events might not get recorded. At large incidence angle, the particles could very like only fly through one PMT or even none of both PMTs (though in this case the angle must be quite large so that $\cos^2$ law is broken anyway). But particles directly from vertical direction are detected as expected. Eventually this distorts the distribution in a way that fluxes around $\theta = 0°$ is untouched but the fluxes at larger angles get suppressed.

A possible future improvement could be just use one PMT as a trigger or these two PMT on one side of straw modules. It will increase noise level but it can presumably improve the distorted angular distribution.

A. Appendix

voltage[V]	counts
1700	541
1700	498
1700	550
1700	519
1750	896
1750	955
1750	1011
1750	985
1800	1412
1800	1437
1800	1478
1800	1515
1850	2531
1850	2375
1850	2362
1850	2426
1900	5092
1900	5137
1900	5066
1900	5086
1950	13 880
1950	14 289
1950	15 100
1950	13 864
2000	19 821
2000	20 246
2000	20 155
2000	20 015

Table 1: Raw data for bottom PMT setup

voltage[V]	counts
2050	22 521
2050	22 788
2050	22 833
2050	22 929
2100	24 609
2100	24 513
2100	24 613
2100	24 371
2150	25 823
2150	25 615
2150	25 877
2150	25 320
2200	26 585
2200	27 102
2200	27 245
2200	26 446
2250	28 292
2250	27 858
2250	27 815
2250	27 451
2300	28 909
2300	28 958
2300	28 576
2300	28 846

Table 2: Raw data for bottom PMT setup (2)

voltage[V]	counts
1700	39
1700	36
1700	44
1700	45
1750	75
1750	78
1750	87
1750	82
1800	156
1800	143
1800	137
1800	148
1850	179
1850	191
1850	229
1850	229
1900	241
1900	231
1900	248
1900	250
1950	286
1950	312
1950	296
1950	280
2000	286
2000	298
2000	331
2000	308

Table 3: Raw data for top PMT setup

voltage[V]	counts
2050	365
2050	345
2050	388
2050	356
2100	413
2100	392
2100	380
2100	409
2150	432
2150	398
2150	385
2150	473
2200	424
2200	436
2200	419
2200	425
2250	409
2250	426
2250	428
2250	396
2300	458
2300	439
2300	411
2300	393

Table 4: Raw data for top PMT setup (2)

References

[1] Prof. H. Pleijel. *Award ceremony speech*. URL: https://www.nobelprize.org/prizes/physics/1936/ceremony-speech/.

[2] Thomas K. Gaiser, Ralph Engel, and Elisa Resconi. *Cosmic rays and particle physics*. Cambridge university press, 2016.

[3] Gabriela Barenboim and Jordi Salvado. "Cosmology and CPT violating neutrinos". In: *The European Physical Journal C* 77.11 (Nov. 2017). ISSN: 1434-6052. DOI: 10.1140/epjc/s10052-017-5347-y. URL: http://dx.doi.org/10.1140/epjc/s10052-017-5347-y.

[4] Claus Grupen et al. *Astroparticle physics*. Springer, 2005.

[5] D.M. Gomez Coral and Arturo Menchaca-Rocha. "SM antideuteron background to indirect dark matter signals in galactic cosmic rays". In: *Journal of Physics: Conference Series* 1602 (July 2020), p. 012005. ISSN: 1742-6596. DOI: 10.1088/1742-6596/1602/1/012005. URL: http://dx.doi.org/10.1088/1742-6596/1602/1/012005.

[6] *Straw Tube Young Student eXperiment - STYX*. URL: https://www.brock.physik.uni-bonn.de/research/styx-experiment.

[7] P.A. Zyla et al. "Review of Particle Physics". In: *PTEP* 2020.8 (2020), p. 083C01. DOI: 10.1093/ptep/ptaa104.

[8] Prashant Shukla and Sundaresh Sankrith. "Energy and angular distributions of atmospheric muons at the Earth". In: *Int. J. Mod. Phys. A* 33.30 (2018), p. 1850175. DOI: 10.1142/S0217751X18501750. arXiv: 1606.06907 [hep-ph].

[9] William R. Leo. *Techniques for nuclear and particle physics experiments*. 2nd. Springer-Verlag Berlin Heidelberg GmbH, 1994.

[10] Unknown. "Lab manual. E217 STYX". In: (2020).

[11] Hermann Kolanoski and Nobert Wermes. *Teilchendetektoren: Grundlagen und Anwendungen*. Springer. ISBN: 978-3-662-45350-6.

[12] CERN. *User Guide: Histograms*. URL: https://root.cern.ch/root/htmldoc/guides/users-guide/Histograms.html.

[13] M. Bahmanabadi. "A method for determining the angular distribution of atmospheric muons using a cosmic ray telescope". In: *Nuclear Instruments and Methods in Physics Research Section A: Accelerators, Spectrometers, Detectors and Associated Equipment* 916 (2019), pp. 1–7. ISSN: 0168-9002. DOI: https://doi.org/10.1016/j.nima.2018.11.010. URL: http://www.sciencedirect.com/science/article/pii/S0168900218315560.